

# HazeSpace2M: A Dataset for Haze Aware Single Image Dehazing

Anonymous Authors

## ABSTRACT

Reducing atmospheric hazes and enhancing image clarity is crucial for a range of applications related to computer vision. The lack of real-life hazy ground truth images necessitates synthetic datasets, which often need more diverse haze types, impeding effective haze type classification and dehazing algorithm selection. This research introduces the HazeSpace2M dataset, a comprehensive collection of over 2 million images designed to enhance the performance of dehazing through haze-type classification. HazeSpace2M includes diverse scenes with 10 haze intensity levels, featuring Fog, Cloud, and a novel category, Environmental Haze (EH). Leveraging the dataset, we introduce a novel technique of haze-type classification followed by specialized dehazers to dehaze hazy images. Unlike the conventional methods, our approach classifies haze types before applying type-specific dehazing, improving clarity and functionality across applications lacking real-life hazy images. We benchmark the state-of-the-art classification models against different combinations of the hazy benchmarking datasets (HBDs) and the Real Hazy Test-set (RHT) from the HazeSpace2M dataset. For instance, ResNet50 and AlexNet, on average, achieve 92.75% and 92.50% accuracy, respectively, against the existing synthetic HBDs. However, the same models furnish 80% and 70% accuracy, respectively, against our RHT, proving the challenging nature of our dataset. Additional experiments utilizing our proposed framework verify that haze-type classification followed by specialized dehazing enhances dehazing results by 2.41% in PSNR, 17.14% in SSIM, and 10.2% in MSE over general dehazers. These results highlight the significance of HazeSpace2M and the proposed framework in addressing the pervasive challenge of atmospheric haze in multimedia processing. The codes and dataset will be available on GitHub soon.

## CCS CONCEPTS

• **Computing methodologies** → **Reconstruction**.

## KEYWORDS

HazeSpace2M, Haze type classification, Haze aware dehazing, Single image dehazing, Haze classification, Atmospheric haze, Multimedia

## 1 INTRODUCTION

Atmospheric haze significantly compromises image clarity, posing difficulties for computer vision tasks in autonomous systems, remote sensing, and surveillance [64]. Adverse weather conditions

that reduce visibility can lead to accidents, as documented in various studies [21, 30, 40, 56]. To tackle the issues of hazes, researchers have developed dehazing algorithms to counteract haze's effects on image quality [7]. Advancements in traffic systems and vehicle detection technology further necessitate enhanced visibility [13, 40, 52, 65]. Current efforts focus on refining models to restore clarity to images impaired by adverse environmental conditions [41, 58, 60]. However, there is a consensus on the necessity for versatile dehazing techniques across variable weather patterns [18], with a rich dataset being crucial for developing robust Convolutional Neural Network-based models for effective atmospheric dehazing.

Large datasets with varied scenes and haze types are scarce; the RESIDE SOTS [32] benchmark dataset covers synthetic hazy images but is limited to a single haze type. Similarly, the Cityscapes [11] dataset includes fog and rain conditions but is confined to street scenes, highlighting a deficit in comprehensive hazy image datasets. Current image restoration (IR) models often operate without recognizing the specific degradation type [31, 36, 42, 43, 57, 61, 63]. Although instruction-based IR methods [8, 10] improve performance by classifying degradation type, they rely on manual input, which is impractical for autonomous systems. An automated model that can identify and adapt to various haze types in the image is needed for effective dehazing without human intervention.

However, to train such versatile models, we need a dataset that offers various haze types across different scene types [18], which is absent in the literature. Identifying this gap in the literature, we develop a dataset named "HazeSpace2M," suitable for haze type classification and training haze type-specific specialized dehazers. We structure the "HazeSpace2M" dataset in a way that is suitable for haze type classification and training haze type-specific specialized dehazers. Leveraging this dataset in this paper, we also propose a novel idea of an intelligent image dehazing approach that performs specialized dehazing based on the haze type present in an input image. Thus, our research makes significant progress in the direction of image dehazing and classification, marked by the following contributions:

- **Development of a Benchmarking Dataset:** We developed HazeSpace2M as a comprehensive benchmarking dataset designed explicitly for haze-type classification in single input images. Additionally, we are the first to introduce a hazy dataset for different scene types, especially the Farmland scene type, which is unparalleled in the literature. This dataset surpasses existing datasets in terms of number of images (over 2 million), scene types, type of hazes, and haze intensity (10 levels).
- **Intelligent Haze Aware Dehazing:** We propose a novel framework that performs dehazing with specialized dehazers based on the haze type present in the input hazy image.
- **Benchmarking SOTA Models:** We evaluate leading classification models, setting new benchmarks for haze-type classification accuracy.

Permission to make digital or hard copies of all or part of this work for personal or professional use, not for profit or commercial advantage and that copies bear this notice and the full citation on the first page. Copyrights for components of this work owned by others than the author(s) must be honored. Abstracting with credit is permitted. To copy otherwise, or to publish, to post on servers or to redistribute to lists, requires prior specific permission and/or a fee. Request permissions from [permissions@acm.org](mailto:permissions@acm.org).

ACM MM, 2024, Melbourne, Australia  
© 2024 Copyright held by the owner/author(s). Publication rights licensed to ACM.  
ACM ISBN 978-x-xxxx-xxxx-x/YY/MM  
<https://doi.org/10.1145/nnnnnnn.nnnnnnn>

- Evidence for Specialized Dehazers' Efficacy: Our findings demonstrate that specialized dehazers, informed by accurate haze type classification, enhance dehazing performance, surpassing the capabilities of generalized dehazing models.

## 2 RELATED WORKS

In recent years, various hazy image datasets [4, 5, 11, 23, 32, 34, 46, 53, 54] have emerged to aid in developing single image dehazing techniques. These datasets offer a range of images affected by different hazes. For instance, the RESIDE dataset [32] encompasses a variety of images, including both indoor and outdoor settings, with hazy conditions and their corresponding ground truth (GT) images. However, it lacks distinct subsets for various types of images and haze conditions. Conversely, the Cityscapes dataset [11] provides fog and rain-afflicted street scenes but lacks variety in scene types. The synthetic image collections FRIDA [54] and FRIDA2 [53] are designed primarily for algorithm assessment in visibility and contrast restoration, encompassing 90 and 330 images across urban road scenes, respectively. Despite their utility, the synthetic nature of these sets limits their effectiveness in modeling the complexity of real-world hazes.

To bridge the above mentioned gaps, the NH Haze [6] dataset, introduced during the NTIRE2020 [1] challenge, features 55 outdoor scenes with actual haze conditions alongside their haze-free GT images, proving invaluable for developing new dehazing methods. Moreover, the Haze4k dataset [34]—split into 3,000 training and 1,000 testing images—provides ample data for benchmarking novel dehazing approaches. Adding diversity, the Kede [37] dataset contains 225 images with nine groups showcasing different outdoor settings and haze thicknesses. In contrast, the O-HAZE [5] dataset with 45 scenes captured under consistent lighting conditions offers realistic pairs of hazy and clear images, facilitating the study of dehazing in authentic environments. In the realm of remote sensing, datasets like Haze1k [23] and RS Haze [46] enrich the dehazing research by providing images categorized by haze density and showcasing a variety of cloud haze levels, respectively. Haze1k offers 900 images curated for remote sensing applications, whereas RS Haze challenges researchers with nine distinct haze levels in its 5,700 GT images. These datasets play a crucial role in enhancing the development of algorithms that deal with the nuances of hazy conditions observed in satellite imagery.

Overall, these datasets have become central to benchmarking the performance of single image dehazing techniques. Especially, the datasets like RESIDE [32] and Foggy Cityscapes [11] with their extensive collection, are excellent for generalizing models and have become a benchmark for assessing dehazing algorithms [9, 14–16, 22, 26, 27, 33, 39, 46, 47]. However, the ranges of haze types and scenes are limited in these datasets, scoping the improvement with more diverse datasets having various haze types for creating classification models capable of classifying various haze conditions. To fill this gap, we present a new dataset that is both broad and diverse, covering a wide range of scene types and haze types, paving the way for breakthroughs in the realm of single image dehazing in terms of developing robust haze type classification and dehazing algorithms.

**Table 1: Overview of HazeSpace2M dataset scene and haze types: annotated with Fog, EH, and Cloud, each with 10 distinct haze intensity levels.**

HazeSpace2M			
Outdoor	Street	Farmland	Satellite
Fog	Fog	Fog	Cloud
EH	EH	EH	
10 different levels of haze for each category			

## 3 OUR DATASET: HAZESPACE2M

HazeSpace2M is a diverse and large dataset with over 2M images, including the GT and Hazy images of three different types of hazes: Fog, Environmental Haze (EH), and Cloud. To the best of our knowledge, we are the first to introduce both EH and Fog separately for scenarios such as Outdoor, Street, and Farmlands. HazeSpace2M is suitable for developing intelligent dehazing models based on haze-type classification.

Notably, the HazeSpace2M includes four main scene categories: Outdoor, Street, Farmland, and Satellite, encompassing three haze conditions: Fog, EH, and Cloud, as stated in Table 1. Each GT image from every scene type features ten corresponding hazy images, varying from low to high intense levels. The HazeSpace2M dataset, curated for research, includes an extensive collection of over 130,193 GT images and approximately two million hazy images, each categorized into distinct levels of haze intensity across various scene types. It also has a subset named Real Hazy Testset (RHT) that features 1,030 real hazy images for evaluating models. This comprehensive dataset not only paves the way for creating more robust dehazing models but also facilitates the development of algorithms capable of classifying the types of haze present, thereby contributing significantly to image processing and multimedia.

**Table 2: Sources and composition of GT in the HazeSpace2M dataset: a breakdown of the various image sources and the number of GT images selected from each source.**

Scene Types	Image Sources	Total # of Images in Source	Total # of GT Images we Pick
Outdoor (OD)	ADE20K [66, 67]	27,638	2,106
	OTS [32]	8,964	7,851
	GSV [62]	62,068	20,696
	SFTGAN [59]	10,200	4,596
	Our Collections	687	687
Street (ST)	GSV [62]	62,068	20,000
	Cityscapes [11]	19,998	19,998
Farmland (FL)	Our Collections	830	830
	Haze1k [23]	1,035	898
Satellite (SL)	Forest Fires [17]	42,815	42,815
	DGLCC [12]	1,146	1,146
	DGRED [? ]	8,570	8,570
<b>Total GT Images:</b>			<b>130,193</b>

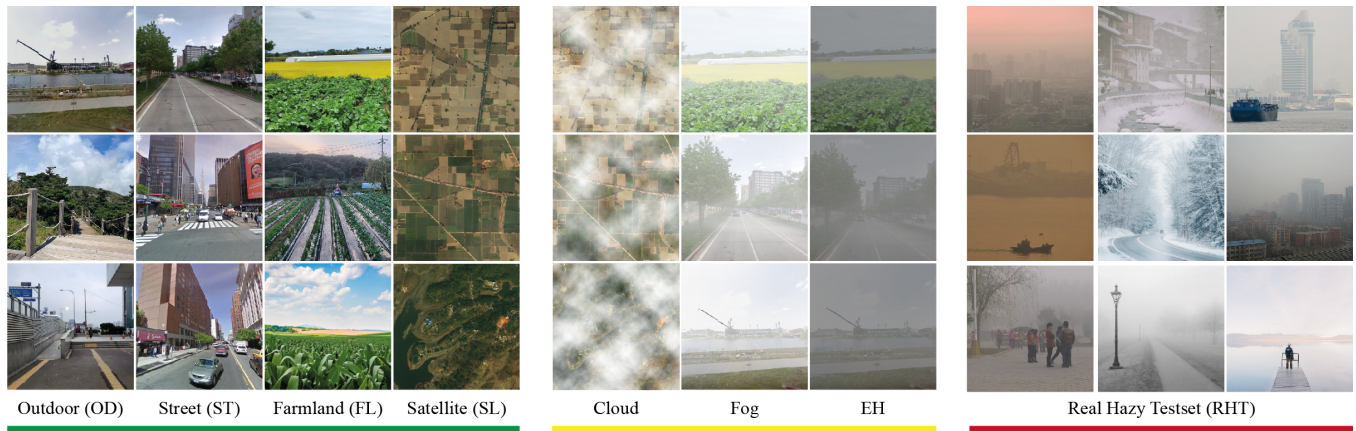


**Figure 1: HazeSpace2M at a glance: Showcasing Ground Truth (Green), Synthetic Hazy (Yellow), and Real Hazy (Red) images across diverse scenes.**

### 3.1 Data Collection and Generation

Before generating the hazy data, we collected a large amount of image data from various sources. These images are mainly the GT images in the HazeSpace2M dataset.

**Quality Assurance.** As shown in Table 2, we collect most of our GT images from the existing datasets or online under a Creative Commons License (CML), and some are the images captured from our personal devices. Cross-checking the quality of these images is a challenging but essential task. Initially, to ensure the quality of the GT images of our HazeSpace2M dataset, we established three conditions for excluding GT images while collecting from different sources. The conditions are as follows:

- **Resolution:** The image is of low quality.
- **Haze Presence:** The image contains haze in any form.
- **Irrelevance:** The image is not relevant to the scene types of HazeSpace2M.

If any image from our sources meets either of these criteria, it is excluded from the GT set of the HazeSpace2M dataset. For example, as shown in Table 2, we selected only 2,106 images from the ADE20k [66, 67] dataset out of 27,638 and 7,851 images out of 8,964 from the RESIDE SOTS [32] to use as GT images in the HazeSpace2M dataset. Similarly, we take 20,000 out of 62,068 images from the GSV [62] dataset as the rest match criteria 3. Thus, we ensure the quality and reusability of the GT images while we collect the GT images for HazeSpace2M from a wide range of sources.

**Scene Types.** As mentioned earlier, our HazeSpace2M dataset comprises diverse scenes. Outdoor images provide aerial and ground-level views of urban environments, capturing elements like architecture and traffic. Street view offers a closer look at urban roads and daily life. Farmland images focus on agricultural areas, detailing rural landscapes. Satellite images from high altitudes afford expansive views of the Earth's valuable surface for geographical and environmental studies and tracking changes in land use patterns, highlighting details unnoticeable at ground level. The images with the green line in Figure 1 display some sample images of different scenes of the HazeSpace2M dataset.

**Haze Types.** The HazeSpace2M dataset features three hazy types: Fog, EH, and Cloud. The haze types are applied to the GT images to create ten different haze intensities, which means that from each GT image, we produce ten hazy images of different haze intensity, which varies from light to dense.

**Fog:** Fog is caused by the presence of water droplets in the air, typically when there is a high relative humidity. It is a ground-level haze that reduces visibility.

**Cloud:** Cloud haze is characterized by cloud formations at various altitudes, affecting the lighting and contrast in images.

**Environmental Haze (EH):** EH is an atmospheric condition characterized by fine particles, aerosols, and pollutants suspended in the air. It is commonly caused by human activities, including industrial emissions and vehicle exhaust, but can also originate from natural sources such as burning from wildfires and agricultural lands. The images with the yellow line in Figure 1 display some sample images of different haze types of the HazeSpace2M dataset.

**Real Hazy Testset (RHT):** The RHT comprises a collection of real-life hazy images sourced online to evaluate the ability of our classification models to identify haze types in real-world scenarios. These images are curated using specific search terms; for instance, searches for "foggy images," "foggy weather," and "winter fog" helped label images as Fog. Similarly, searches using "environmental haze," "air pollution," "wildfire," and "smoky environment" facilitated the labeling of images as EH. We meticulously verify each image's visual characteristics and origin to accurately represent the specified haze type. Thus, we collected around 686 images with fog haze and 344 with EH. The images with the red line in Figure 1 present some sample images of the RHT subset of the HazeSpace2M dataset. However, sourcing original satellite images depicting cloud haze posed a challenge. To address this, we incorporated 500 satellite cloudy images from the RS Haze [46] dataset into RHT, enabling comprehensive evaluation of the classification models trained on the HazeSpace2M dataset.

**Table 3: Details of the subdivision of the HazeSpace2M dataset according to scene types and haze conditions, listing the number of GT images and the generated hazy images across different subsets with the defined names for each subset.**

Subset Names of HazeSpace2M depending on various Scene Types	Subsets Names of HazeSpace2M depending on various Haze Types	Nature of the Image	HazeSpace2M	
			# of GT Images	# of Hazy Images
Outdoor (OD)	Outdoor Fog (ODF) Outdoor Environmental Haze (ODEH)	Synthetic Synthetic	35,936	359,360 359,360
Street (ST)	Street Fog (STF) Street Environmental Haze (STEH)	Synthetic Synthetic	39,998	399,980 399,980
Farmlands (FL)	Farmland Fog (FLF) Farmland Environmental Haze (FLEH)	Synthetic Synthetic	830	8,300 8,300
Satellite (SL)	Satellite Cloud (SLC)	Satellite	53,429	534,290
<b>Real Haze Testset (RHT)</b>	-	Real	-	1,030
<b>Total:</b>			<b>130,193</b>	<b>2,070,600</b>
<b>Total # of Images (GT + Hazy) in HazeSpace2M dataset:</b>			<b>2,200,793 (2.2 Million Images)</b>	

**Table 4: Comparative evaluation of image quality metrics across the existing datasets. The comparison of PSNR and SSIM values for the lowest and highest haze levels across different datasets, including our HazeSpace2M dataset.**

Datasets	Scene Type	Haze types			# of GT Images	# of Hazy Images	Lowest Haze Level		Highest Haze Level	
		Fog	Cloud	EH			PSNR ↑	SSIM ↑	PSNR ↑	SSIM ↑
FRIDA [53, 54]	Outdoor	✓	×	×	84	420	27.54	0.81	29.92	0.69
Foggy Driving [11]	Street	✓	×	×	10,425	10,425	28.50	0.88	27.70	0.68
I-Haze [34]	Outdoor	Not Specified			30	30	29.34	0.85	27.57	0.48
O-Haze [46]	Satellite	Not Specified			45	45	28.96	0.80	27.49	0.37
SOTS [32]	Outdoor	Not Specified			8,964	313,950	29.27	<b>0.99</b>	27.44	0.83
NH Haze [6]	Outdoor	Non-Homogenous			55	55	28.43	0.66	27.70	<b>0.22</b>
Haze1k [23]	Satellite	×	✓	×	1,035	1,035	28.51	0.91	27.49	<u>0.23</u>
RS Haze [46]	Satellite	×	✓	×	6,000	54,000	27.57	0.97	27.27	0.52
<b>HazeSpace2M</b>	Outdoor	✓	×	✓	35,936	<b>718,720</b>	30.91	<u>0.98</u>	<u>27.11</u>	0.25
	Street	✓	×	✓	39,998	<u>799,960</u>	31.91	<u>0.98</u>	27.36	0.39
	<b>Farmland</b>	✓	×	✓	830	16,600	<b>32.32</b>	0.97	<b>27.08</b>	<u>0.23</u>
	Satellite	×	✓	×	53,429	534,290	<b>34.61</b>	<u>0.98</u>	27.49	<u>0.23</u>

### 3.2 Annotation Process and Tools

Inspired by [23] and [46], we utilized Adobe Photoshop 25.1 with its advanced ML-based Neural Filters (NFs) to generate hazy images for our HazeSpace2M dataset [2]. We crafted Photoshop actions, which automate editing tasks, to create varied haze levels [3]. This approach allowed the efficient processing of our extensive dataset, consisting of over two million images, generated over several months using three computers.

### 3.3 Quantitative Analysis

The HazeSpace2M dataset, as shown in Table 3, incorporates Fog and EH hazing on its Outdoor (OD), Street (ST), and Farmland (FL) subsets, while the Satellite (SL) subset is treated with Cloud haze, creating subsets designated as ODF, STF, FLF for Fog; ODEH, STEH, FLEH for EH; and SLC for Cloud haze. The OD, ST, FL, and SL subsets consist of synthetic hazy images alongside RFH and REH, which are real hazy images. Fog and EH haze types applied across ten intensity levels to the OD subset’s 35,936 GT images result in 718,720 hazy images for OD, equally split between ODF and ODEH. The ST and FL subsets yield 816,560 hazy images from 40,828 GT images, and SL comprises 534,290 Cloud-hazy images from 53,429

GT images. Totalling around 130,193 GT images, the HazeSpace2M spans approximately 2.2 million hazy images when considering all three haze types and ten haze intensities per GT image, detailed in Table 3.

Compared to established datasets in literature [4–6, 11, 23, 32, 46, 53, 54], Table 4 presents the comparative PSNR and SSIM metrics. The HazeSpace2M dataset demonstrates high PSNR and SSIM at the lowest haze level, reflecting clear images under minimal hazing. At the highest haze level, these metrics show a marked reduction, illustrating the substantial impact of intense hazing. This variance signifies the dataset’s wide range of haze intensities, providing a broader scope for analysis than previous datasets. The HazeSpace2M also exceeds others in image volume, offering an extensive array of GT and hazy images. Including the FL subset introduces a new scene type to the dataset, enriching the diversity and research applicability. Comparing the scene types and the haze types, it is evident that the HazeSpace2M consists of a diverse type of scene and haze compared to the existing haze image datasets. Each subset within HazeSpace2M contains GT and hazy images, establishing its superiority in dataset quantity and scene variety.

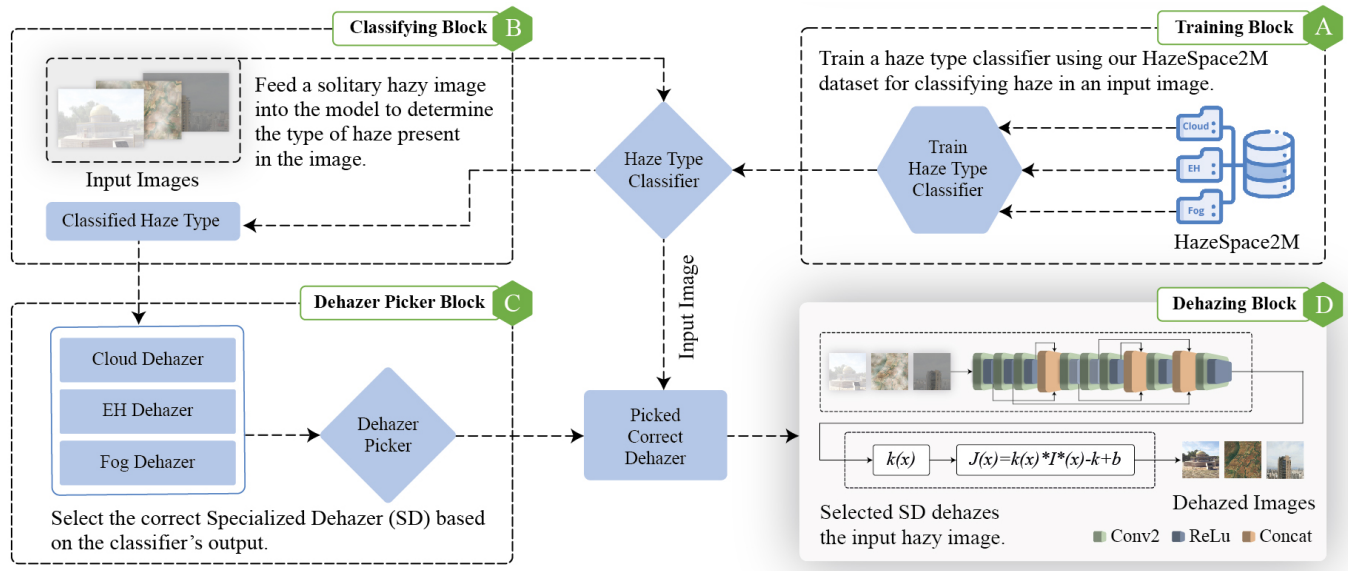


Figure 2: Our proposed framework for specialized dehazer-based intelligent dehazing based on the haze type classification in image enhancement workflows, including (A) training classifiers to recognize haze types, (B) using the classifier to identify the type of haze in a single input image, (C) selecting the appropriate dehazer based on the haze classification, and (D) the final dehazing process to clear the image from atmospheric obscurations with the selected specialized dehazer.

## 4 PROPOSED FRAMEWORK

Our proposed approach for intelligent dehazing based on haze type classification is illustrated in Figure 2. It has four main blocks, each with a particular task. As shown in Figure 2A, we use the dataset to train the SOTA classification models [19, 20, 24, 25, 28, 35, 38, 44, 45, 48–51] to sort out the models that could classify haze in the single-input image. Thus, we benchmark the SOTA models against the existing synthetic hazy benchmarking datasets and the Real Hazy Testset of the HazeSpace2M. Then, as illustrated in Figure 2B, we use the trained classifier for classifying the haze in a single input image. In this paper, we train the SOTA classification models on the HazeSpace2M dataset for haze-type classification. As in Figure 2C block, based on the classification result and output haze type, the model selects a suitable dehazer and performs the inference accordingly in the Inference Block, which is illustrated in Figure 2D. As with the classification models, we train three dehazing algorithms for three different hazes, namely Fog, EH, and Cloud, on our HazeSpace2M dataset. These dehazers are trained based on the modified ASM [55] in 100 epochs. Utilizing these three specialized dehazers, the complete framework we propose for specialized dehazers-based intelligent dehazing based on the haze type classification is depicted in Figure 2.

### 4.1 Experimental Setups

We conduct several experiments in line with the methodology illustrated in Figure 2. Our focus begins with training and evaluating classification models, followed by assessing generalized and specialized dehazers using the HazeSpace2M dataset.

**Haze Type Classification.** For training and validating the classification models, we take subsets from the HazeSpace2M dataset and split them as follows:

**Train and Validation Dataset:** We train our models using a subset of 15,000 images from the HazeSpace2M dataset, evenly divided among the three haze types, with 5,000 images for each category. We allocate 85% of these images for training (12,750) and the remaining 15% (2,250) for validation.

**Test Dataset:** We assess models on synthetic and real-life hazy images, creating different sets of testing datasets using the existing Hazy Benchmarking Datasets (HBDs) [5, 11, 23, 32, 46, 53, 54]. We also test the models against the RHT subset of the HazeSpace2M.

To ensure uniform training, all models used a batch size 32, a 0.001 learning rate, and a 512-pixel resolution. Following the footsteps of DTMIC [29], each model underwent a 50-epoch training with a 10-step patience early stopping technique.

**Single Image Dehazing.** We introduce two terms, namely Specialized Dehazer and Generalized Dehazer, and defined below to differentiate between the training processing for each.

**Specialized Dehazer (SD):** This term refers to a dehazing model explicitly trained on images of a particular type of haze. For instance, a model trained exclusively on foggy images to dehaze fog-related obscurities is considered an SD.

**Generalized Dehazer (GD):** In contrast, the Generalized Dehazing model is trained on a broader spectrum of hazy images. The GD model is not limited to a specific type of haze but is designed to handle various hazy conditions.

To conduct experiments with both SD and GD, we utilize the same dehazer architecture as depicted in Figure 2D. This architecture is developed based on the modified Atmospheric Scattering

**Table 5: Performance evaluation of the SOTA models using accuracy (ACC), precision (PRE), and recall (REC) against different combinations of the Hazy Benchmarking Datasets (HBDs), highlighting their effectiveness for haze type classification. These models are trained on the HazeSpace2M dataset.**

Models	Different Combinations of Hazy Benchmarking Datasets for Haze Type Classification												Average ACC
	Fog: FRIDA			Fog: Cityscapes			Fog: Cityscapes			Fog: Cityscapes			
	EH: O-Haze			EH: NH-Haze			EH: NH-Haze			EH: O-Haze			
	Cloud: Haze1k			Cloud: Haze1k			Cloud: RS-Haze			Cloud: Haze1k			
ACC	PRE	REC	ACC	PRE	REC	ACC	PRE	REC	ACC	PRE	REC		
AlexNet	0.96	0.96	0.96	0.95	0.95	0.95	<u>0.83</u>	0.91	0.83	<u>0.96</u>	0.96	0.96	<u>92.50</u>
ConvNextLarge	0.88	0.93	0.88	0.86	0.92	0.86	0.80	0.93	0.80	0.88	0.94	0.88	85.50
DenseNet121	<b>0.98</b>	0.98	0.98	0.90	0.96	0.90	0.63	0.95	0.63	0.90	0.97	0.90	85.25
DenseNet161	0.91	0.92	0.91	0.89	0.95	0.89	0.68	0.87	0.68	0.88	0.94	0.88	84.00
DenseNet169	0.94	0.93	0.94	0.94	0.95	0.94	0.73	0.87	0.73	0.93	0.95	0.93	88.50
DenseNet201	0.96	0.96	0.96	<b>0.96</b>	0.96	0.96	0.78	0.94	0.78	<b>0.97</b>	0.97	0.97	91.75
EfficientNet_B0	0.88	0.95	0.88	0.85	0.95	0.85	0.63	0.92	0.63	0.85	0.96	0.85	80.25
EfficientNetV2Large	0.90	0.93	0.90	0.87	0.91	0.87	0.65	0.88	0.65	0.88	0.93	0.88	82.50
GoogleNet	0.86	0.86	0.86	0.88	0.89	0.88	0.74	0.86	0.74	0.89	0.90	0.89	84.25
Inception_V3	0.78	0.86	0.78	0.79	0.89	0.79	0.68	0.90	0.68	0.80	0.91	0.80	76.25
MNasNet	0.94	0.95	0.94	0.82	0.94	0.82	0.52	0.93	0.52	0.82	0.95	0.82	77.50
MobileNetV2	0.92	0.95	0.92	0.80	0.95	0.80	0.70	0.96	0.70	0.81	0.96	0.81	80.75
MobileNetV3	0.76	0.94	0.76	0.51	0.92	0.51	0.43	0.95	0.43	0.51	0.94	0.51	55.25
<b>ResNet50</b>	0.96	0.96	0.96	<u>0.95</u>	0.94	0.95	<b>0.84</b>	0.92	0.84	<u>0.96</u>	0.96	0.96	<b>92.75</b>
ResNet101	<b>0.98</b>	0.98	0.98	0.94	0.96	0.94	0.78	0.92	0.78	0.94	0.95	0.94	91.00
ResNet152	<u>0.97</u>	0.97	0.97	0.94	0.96	0.94	0.76	0.93	0.76	0.94	0.96	0.94	90.25
ShuffleNetV2	0.86	0.87	0.86	0.90	0.91	0.90	0.76	0.94	0.76	0.90	0.91	0.90	85.50
SqueezeNet1	0.96	0.96	0.96	0.90	0.94	0.90	0.71	0.96	0.71	0.91	0.96	0.91	87.00
VGG16	0.95	0.94	0.95	0.93	0.92	0.93	<b>0.84</b>	0.92	0.84	0.95	0.94	0.95	91.75

**Table 6: Evaluation of the SOTA models against the Real Hazy Testset (RHT) of the HazeSpace2M dataset using accuracy (ACC), precision (PRE), and recall (REC).**

Models	ACC	PRE	REC
AlexNet	<u>0.70</u>	0.71	<u>0.70</u>
ConvNextLarge	0.63	0.72	0.63
DenseNet121	0.46	0.69	0.46
DenseNet161	0.58	0.67	0.58
DenseNet169	0.56	0.65	0.56
DenseNet201	0.68	0.71	0.68
EfficientNet_B0	0.49	0.64	0.49
EfficientNetV2Large	0.48	0.67	0.48
GoogleNet	0.66	0.68	0.66
Inception_V3	0.54	0.63	0.54
MNasNet	0.45	0.68	0.45
MobileNetV2	0.60	0.71	0.60
MobileNetV3	0.60	0.71	0.60
<b>ResNet50</b>	<b>0.80</b>	<b>0.78</b>	<b>0.80</b>
ResNet101	<u>0.70</u>	0.72	0.70
ResNet152	0.63	0.71	0.63
ShuffleNetV2	0.67	0.72	0.67
SqueezeNet1	0.65	<u>0.73</u>	0.65
VGG16	<u>0.70</u>	0.69	<u>0.70</u>

Model (ASM) [55] for removing haze in a single input image as follows:

$$I(x) = J(x) \times t(x) + A \times (1 - t(x)). \quad (1)$$

The term  $K(x)$  represents a combined variable that encapsulates both  $t(x)$  and  $A$ , while  $I(x)$  signifies the observed image with haze. Here,  $A$  is the global atmospheric light and  $t(x)$  is the transmission map defined as:

$$t(x) = e^{-\beta d(x)}, \quad (2)$$

where  $\beta$  is the scattering coefficient of the atmosphere, and  $d(x)$  is the distance between the object and the camera. The modified version of Eq. (1) that is proposed for LDNet gives improved performance for removing haze from the images, which is verified through comprehensive inferences on different datasets [55]. Hence, for the experiments in our paper, we employ the modified version of the ASM model that is stated as follows:

$$J(x) = K(x) \times I(x) - K(x) + b_{\text{bias}}, \quad (3)$$

where the bias term is incorporated with a default value of 1 and the encapsulated values of  $t(x)$  and  $A$ , which we define by  $K(x)$ , as:

$$K(x) = \frac{\frac{1}{t(x)} \times (I(x) - A) + (A - b_{\text{bias}})}{(I(x) - 1)}. \quad (4)$$

For the experiments of single image dehazing and to know if SD performs better than GD, we use LDNet [55] that is developed based on Eq. (3) with the same hyperparameter settings as the backbone of our dehazer algorithms and train them with our mentioned training datasets in different steps as:

- LDNet: Trained using the RESIDE [32] dataset, a common benchmark in dehazing research.

- GDNets: Trained on a composite dataset of 150,000 images comprising images affected by Fog, Cloud, and EH to create a generalized model.
- SDNets: Individually trained on distinct haze types. Initially, the model is trained exclusively on Fog type hazy images, followed by training on Cloud type, and finally on EH type hazy images, with each model saved after training.

With these setups of the dehazers mentioned above, we organize the training, validation, and test datasets in the following manner:

**Train and Validation Dataset:** For the SD models, each targeting a specific haze type (Fog, EH, and Cloud), we select 5,000 GT images and their 50,000 corresponding hazy images at ten distinct intensity levels from each class within the HazeSpace2M dataset. Consequently, we train each SD model using these 50,000 hazy images. In contrast, for the GD model, we amalgamate the 50,000 hazy images from each of the three classes, resulting in a comprehensive dataset of 150,000 hazy images encompassing all haze types. In both scenarios, we divide the dataset into training and validation sets with a 90/10 split ratio, ensuring a balanced model training and validation approach.

**Test Dataset:** To evaluate the performance of the SD and GD models for different types of hazes, we curated a test subset from the HazeSpace2M dataset with the images unseen to the model. This subset comprises 1,000 hazy images for each haze category, distributed across ten distinct intensity levels. This test dataset verifies the models' robustness and effectiveness in handling a broad spectrum of haze types and varying levels of haze intensity.

## 5 EXPERIMENTAL RESULTS

Our dual experiments, single haze type classification, and dehazing for a single input image demonstrate the HazeSpace2M dataset's versatility and wide-ranging applicability. The experimental results of both experiments are discussed in the following sections.

### 5.1 Results of Haze Type Classification

Our evaluation of SOTA classification models on both synthetic and real hazy images commenced with a training phase of 50 epochs, subsequently assessing performance on the HBDs and RHT datasets are presented in Table 5 and Table 6. Initial results highlighted the challenge within the RHT subset, as most models fell short of achieving 80% accuracy. Nonetheless, ResNet50 surpassed this benchmark, showcasing its potential for single image haze type classification despite being only trained for a short period and training with a subset of the HazeSpace2M dataset.

Expanding our investigation, as stated in Table 5, some of the SOTA models namely AlexNet, DenseNet201, ResNet50, ResNet101, ResNet152, and VGG16 give over 90% accuracy on average against the different combinations of HBDs, while models like Inception\_V3, MNasNet, MobileNetV3 give 70% accuracy below on average. The bold values for each accuracy (ACC) column represent the top accuracy among all the accuracies while testing the models against the corresponding combinations of the HBDs, while the underlined values represent the second-highest accuracies. The average ACC column shows the average accuracy achieved by each model against the HBDs. Exploring this column, we find that the AlexNet achieves an accuracy of 92.50%, while ResNet50 outperforms the AlexNet

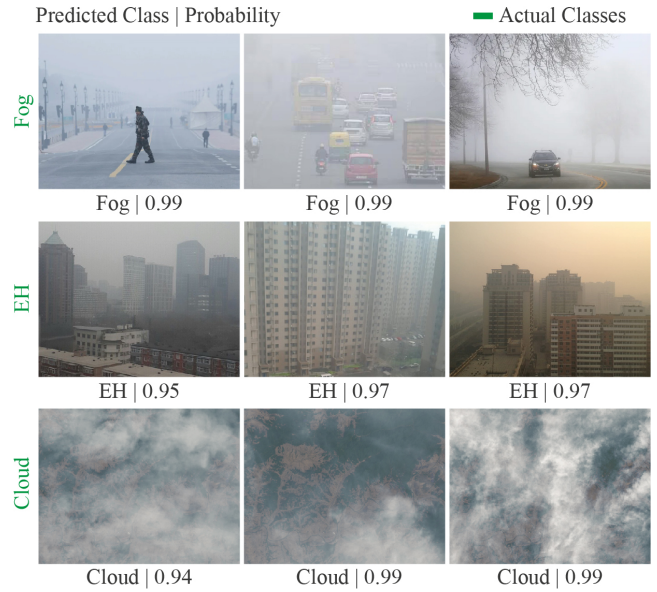


**Figure 3: Sample images from the Real Hazy Testset (RHT) for which the haze type is correctly classified by ResNet50, along with the prediction probabilities.**

with a slightly improved accuracy of 92.75%. Analyzing all these facts, we observed that ResNet50 and AlexNet performed robustly throughout the testing of different combinations of the HBDs.

We further evaluate all the models against the RHT to observe the performance of these models on images affected by the real atmospheric haze. As presented in Table 6, we still found ResNet50 to outperform the other models with an accuracy of 80%, while AlexNet, ResNet101, and VGG16 achieved 70% accuracy.

While several models result in very good accuracy on the synthetic datasets and very low accuracy on the RHT, the challenge lies in classifying haze types on a real hazy image. The ResNet50 shows some robustness by giving 80% accuracy, while the other models failed. The inference results on the RHT images are presented in the Figure 3, showing some of the correctly classified RHT images by the ResNet50 model. Overall, the results show the need to develop robust classification models that can outperform the existing SOTA models in the context of atmospheric haze-type classification.

### 5.2 Results of Single Image Dehazing

To investigate the effectiveness of SD models compared to GD models in single image dehazing, we conducted extensive evaluations using the HazeSpace2M dataset. Our methodology involved training the LDNet [55] model and its SD and GD variants across three distinct stages.

Our study rigorously evaluated the original LDNet dehazing model, achieving average PSNR, SSIM, and MSE values of 28.15, 0.65, and 99.89, respectively. We based these averages on comprehensive testing against various haze types, having 1000 hazy images for each haze type with detailed results outlined in Table 7.

Similarly, our evaluation of the GDNets and SDNets models on identical test sets, as detailed in Table 7, reveals that the SD models

**Table 7: Comparative performance metrics for LDNet, GDNet, and SDNets using PSNR, SSIM, and MSE scores for each model when subjected to dehazing tasks across various hazy conditions represented in fog, EH, and cloud test sets. The average scores reflect the overall performance of each model in processing unknown hazy images.**

Testsets	LDNet			GDNet			SDNets		
	PSNR $\uparrow$	SSIM $\uparrow$	MSE $\downarrow$	PSNR $\uparrow$	SSIM $\uparrow$	MSE $\downarrow$	PSNR $\uparrow$	SSIM $\uparrow$	MSE $\downarrow$
<b>Fog Testset</b>	28.47	0.78	92.46	28.47	0.77	92.31	<b>28.55</b>	<b>0.85</b>	<b>90.49</b>
<b>EH Testset</b>	27.89	0.44	105.44	27.93	0.63	104.78	<b>28.34</b>	<b>0.79</b>	<b>98.43</b>
<b>Cloud Testset</b>	28.11	0.75	101.76	28.29	0.70	97.85	<b>29.84</b>	<b>0.83</b>	<b>76.17</b>
<b>Average</b>	28.15	0.65	99.89	<u>28.23</u>	<u>0.70</u>	<u>98.31</u>	<b>28.91 (2.41%+)</b>	<b>0.82 (17.14%+)</b>	<b>88.36 (10.12%+)</b>

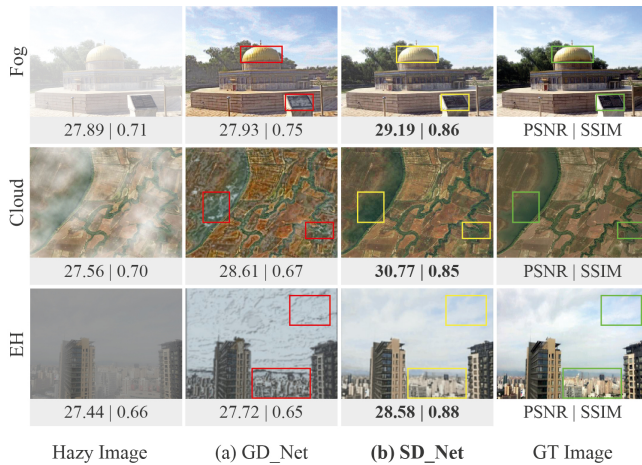


**Figure 4: Visual comparison of image dehazing results from LDNet, GDNet, and SDNet, with PSNR and SSIM metrics highlighted for clarity. Ground truth images are shown for reference, demonstrating the dehazing quality and the practical application of our proposed framework.**

surpass both the LDNet and GDNet in performance. The SDNet models demonstrate PSNR, SSIM, and MSE values of 28.91, 0.82, and 88.36, outperforming the GDNet, which records 28.23, 0.70, and 98.31.

The PSNR values show an improvement of around 2.7% for LDNet compared to SDNets. Similarly, the performance of SDNets improved by 2.4% over GDNet considering the PSNR values from the experimental results presented in Table 7. Moreover, when we examine the SSIM and MSE values, we see a clear performance difference among these models. For example, the SDNets yield around 26.15% higher SSIM and 23.75% improved MSE than the original LDNet. Similarly, compared to the GDNet, the SDNet models show an increase of around 17.14% in SSIM and 10.12% enhancement in MSE for dehazing images affected by Fog, EH, and Cloud. The SDNets outperform the other two models in all three metrics with a PSNR of 28.91, SSIM of 0.82, and MSE of 88.36, showing the effectiveness of an SD model over a GD model.

In addition to comparing performance metrics, the visual examination reveals the superiority of the SD model over the GD models. The single image dehazing examples in Figure 4 demonstrate the visual clarity achieved by the SD model is markedly better than

that produced by the original LDNet [55] and GDNet. Figure 4(c) presents the dehazed images of different haze types using the SDNet models. On the other hand, the inference results of the LDNet and GDNet, which we train traditionally with a relatively larger dataset, have been presented in Figure 4(a & b). To compare the visual clarity of the output images from each model, we highlight the differences via the rectangles. Considering PSNR and SSIM, the SDNet models give higher values than both traditional models, where LDNet has trained on RESIDE [32] dataset, and GDNet is trained on a subset of the HazeSpace2M dataset. We ran the inference on the images unknown to the models, i.e., we did not use these images to train the models. It should be noted that the training sets for the SDNet models are 50,000 images, whereas the training set for the GDNet model is 150,000. Even though we train the GDNet model with 3 $\times$  more different haze types images, SDNets outperform GDNet, ensuring the superiority of our proposed framework.

This data conclusively supports the superiority of specialized dehazers-based dehazing techniques in enhancing single image dehazing. The clear implication is that classifying the type of haze in an image (as illustrated in Figure 2B) and subsequently applying the appropriate dehazing technique (Figure 2C) boosts the dehazing model's efficacy. Here, the Novel HazeSpace2M dataset leads the way by offering a diverse, large, and challenging hazy dataset with the confirmation of haze type classification, which results in better dehazing.

## 6 CONCLUSION

This paper introduces HazeSpace2M, an extensive dataset of over 2 million images designed to introduce haze-type classification and specialized dehazer-based image dehazing, addressing a critical need in computer vision for autonomous systems and security applications. While our computational resources limited training with the entire dataset, leading to reliance on partial datasets for model training, our results confirm HazeSpace2M's effectiveness in real-world haze condition classification, particularly highlighted by the RHT subset performance. Future efforts will focus on expanding the dataset's diversity in haze types, depths, and intensities and benchmarking dehazing models to fully leverage HazeSpace2M's potential. Our study demonstrates the significant role of accurate haze type classification in enhancing dehazing outcomes, offering a promising path forward for precision in image processing under adverse weather conditions, thereby filling a crucial gap in the field and setting the stage for future advancements.

## REFERENCES

- [1] Abdelrahman Abdelhamed, Mahmoud Afifi, Radu Timofte, and Michael S Brown. 2020. Ntire 2020 challenge on real image denoising: Dataset, methods and results. In *Proceedings of the IEEE/CVF Conference on Computer Vision and Pattern Recognition Workshops*. 496–497.
- [2] Adobe. 2024. *Explore a range of creativity with Neural Filters*. Retrieved April 11, 2024 from <https://helpx.adobe.com/content/help/en/photoshop/using/neural-filters.html>
- [3] Adobe. 2024. *Learn how to access various default actions available in Photoshop*. Retrieved April 11, 2024 from <https://helpx.adobe.com/photoshop/using/actions-actions-panel.html>
- [4] Cosmin Ancuti, Codruta O Ancuti, Radu Timofte, and Christophe De Vleeschouwer. 2018. I-HAZE: A dehazing benchmark with real hazy and haze-free indoor images. In *Advanced Concepts for Intelligent Vision Systems: 19th International Conference, ACIVS 2018, Poitiers, France, September 24–27, 2018, Proceedings 19*. Springer, 620–631.
- [5] Codruta O Ancuti, Cosmin Ancuti, Radu Timofte, and Christophe De Vleeschouwer. 2018. O-haze: a dehazing benchmark with real hazy and haze-free outdoor images. In *Proceedings of the IEEE conference on computer vision and pattern recognition workshops*. 754–762.
- [6] Codruta O Ancuti, Cosmin Ancuti, Florin-Alexandru Vasluianu, and Radu Timofte. 2020. Ntire 2020 challenge on nonhomogeneous dehazing. In *Proceedings of the IEEE/CVF Conference on Computer Vision and Pattern Recognition Workshops*. 490–491.
- [7] Codruta O Ancuti, Cosmin Ancuti, Florin-Alexandru Vasluianu, Radu Timofte, Han Zhou, Wei Dong, Yangyi Liu, Jun Chen, Huan Liu, Liangyan Li, et al. 2023. NTIRE 2023 HR nonhomogeneous dehazing challenge report. In *Proceedings of the IEEE/CVF Conference on Computer Vision and Pattern Recognition*. 1808–1825.
- [8] Tim Brooks, Aleksander Holynski, and Alexei A Efros. 2023. Instructpix2pix: Learning to follow image editing instructions. In *Proceedings of the IEEE/CVF Conference on Computer Vision and Pattern Recognition*. 18392–18402.
- [9] BSNV Chaitanya and Snehasis Mukherjee. 2021. Single image dehazing using improved cycleGAN. *Journal of Visual Communication and Image Representation* 74 (2021), 103014.
- [10] Marcos V Conde, Gregor Geigle, and Radu Timofte. 2024. High-Quality Image Restoration Following Human Instructions. *arXiv preprint arXiv:2401.16468* (2024).
- [11] Marius Cordts, Mohamed Omran, Sebastian Ramos, Timo Rehfeld, Markus Enzweiler, Rodrigo Benenson, Uwe Franke, Stefan Roth, and Bernt Schiele. 2016. The cityscapes dataset for semantic urban scene understanding. In *Proceedings of the IEEE conference on computer vision and pattern recognition*. 3213–3223.
- [12] Ilke Demir, Krzysztof Koperski, David Lindenbaum, Guan Pang, Jing Huang, Saikat Basu, Forest Hughes, Devis Tuia, and Ramesh Raskar. 2018. DeepGlobe 2018: A Challenge to Parse the Earth Through Satellite Images. In *The IEEE Conference on Computer Vision and Pattern Recognition (CVPR) Workshops*.
- [13] Vidhi Desai, Sheshang Degadwala, and Dhairya Vyas. 2023. Multi-categories vehicle detection for urban traffic management. In *2023 Second International Conference on Electronics and Renewable Systems (ICEARS)*. IEEE, 1486–1490.
- [14] Bosheng Ding, Ruiheng Zhang, Lixin Xu, Guanyu Liu, Shuo Yang, Yumeng Liu, and Qi Zhang. 2023. U 2 D 2 Net: Unsupervised unified image dehazing and denoising network for single hazy image enhancement. *IEEE Transactions on Multimedia* (2023).
- [15] Akshay Dudhane, Prashant W Patil, and Subrahmanyam Murala. 2020. An end-to-end network for image de-hazing and beyond. *IEEE Transactions on Emerging Topics in Computational Intelligence* 6, 1 (2020), 159–170.
- [16] Masud An-Nur Islam Fahim and Ho Yub Jung. 2020. Single image dehazing using end-to-end deep-dehaze network. In *The 9th International Conference on Smart Media and Applications*. 158–163.
- [17] Open Data Canada Government of Canada. 2024. *Forest Fires*. Retrieved April 11, 2024 from <https://open.canada.ca/data/en/dataset/9d8f219c-4df0-4481-926f-8a2a532ca003>
- [18] Jie Gui, Xiaofeng Cong, Yuan Cao, Wenqi Ren, Jun Zhang, Jing Zhang, Jiuxin Cao, and Dacheng Tao. 2023. A comprehensive survey and taxonomy on single image dehazing based on deep learning. *Comput. Surveys* 55, 13s (2023), 1–37.
- [19] Kaiming He, Xiangyu Zhang, Shaoqing Ren, and Jian Sun. 2016. Deep residual learning for image recognition. In *Proceedings of the IEEE conference on computer vision and pattern recognition*. 770–778.
- [20] Andrew Howard, Mark Sandler, Grace Chu, Liang-Chieh Chen, Bo Chen, Mingxing Tan, Weijun Wang, Yukun Zhu, Ruoming Pang, Vijay Vasudevan, et al. 2019. Searching for mobilenetv3. In *Proceedings of the IEEE/CVF international conference on computer vision*. 1314–1324.
- [21] H. Howard, J. McKinley, and A. Elkeurti. 2024. *Wildfire Smoke: Smoky Air Disrupts Life in the Northeast - The New York Times*. Retrieved April 11, 2024 from <https://www.nytimes.com/live/2023/06/07/us/canada-wildfires-air-quality-smoke#heres-the-latest-on-the-worsening-air-quality-in-the-us>
- [22] Cheng-Hsiung Hsieh and Ze-Yu Chen. 2023. Using Haze Level Estimation in Data Cleaning for Supervised Deep Image Dehazing Models. *Electronics* 12, 16 (2023), 3485.
- [23] Binghui Huang, Li Zhi, Chao Yang, Fuchun Sun, and Yixu Song. 2020. Single satellite optical imagery dehazing using SAR image prior based on conditional generative adversarial networks. In *Proceedings of the IEEE/CVF winter conference on applications of computer vision*. 1806–1813.
- [24] Gao Huang, Zhuang Liu, Laurens Van Der Maaten, and Kilian Q Weinberger. 2017. Densely connected convolutional networks. In *Proceedings of the IEEE conference on computer vision and pattern recognition*. 4700–4708.
- [25] Forrester N Iandola, Song Han, Matthew W Moskewicz, Khalid Ashraf, William J Dally, and Kurt Keutzer. 2016. SqueezeNet: AlexNet-level accuracy with 50x fewer parameters and < 0.5 MB model size. *arXiv preprint arXiv:1602.07360* (2016).
- [26] RS Jaisurya and Snehasis Mukherjee. 2023. AGLC-GAN: Attention-based global-local cycle-consistent generative adversarial networks for unpaired single image dehazing. *Image and Vision Computing* 140 (2023), 104859.
- [27] Zheyang Jin, Shiqi Chen, Yueting Chen, Zhihai Xu, and Huajun Feng. 2023. Let segment anything help image dehaze. (2023). *arXiv:arXiv preprint arXiv:2306.15870*
- [28] Alex Krizhevsky, Ilya Sutskever, and Geoffrey E Hinton. 2012. Imagenet classification with deep convolutional neural networks. *Advances in neural information processing systems* 25 (2012).
- [29] Sanjeev Kumar and B Janet. 2022. DTMIC: Deep transfer learning for malware image classification. *Journal of Information Security and Applications* 64 (2022), 103063.
- [30] W. Lanzoni and A. L. Matthews. 2024. *What does the sky look like when wildfire smoke is hazardous?* | CNN. Retrieved April 11, 2024 from <https://edition.cnn.com/air-quality-wildfire-smoke-pollution-dg/index.html>
- [31] Boyun Li, Xiao Liu, Peng Hu, Zhongqin Wu, Jiancheng Lv, and Xi Peng. 2022. All-in-one image restoration for unknown corruption. In *Proceedings of the IEEE/CVF Conference on Computer Vision and Pattern Recognition*. 17452–17462.
- [32] Boyi Li, Wenqi Ren, Dengpan Fu, Dacheng Tao, Dan Feng, Wenjun Zeng, and Zhangyang Wang. 2018. Benchmarking single-image dehazing and beyond. *IEEE Transactions on Image Processing* 28, 1 (2018), 492–505.
- [33] Yuenan Li, Yuhang Liu, Qixin Yan, and Kuangshi Zhang. 2020. Deep dehazing network with latent ensembling architecture and adversarial learning. *IEEE Transactions on Image Processing* 30 (2020), 1354–1368.
- [34] Ye Liu, Lei Zhu, Shunda Pei, Huazhu Fu, Jing Qin, Qing Zhang, Liang Wan, and Wei Feng. 2021. From synthetic to real: Image dehazing collaborating with unlabeled real data. In *Proceedings of the 29th ACM international conference on multimedia*. 50–58.
- [35] Zhuang Liu, Hanzi Mao, Chao-Yuan Wu, Christoph Feichtenhofer, Trevor Darrell, and Saining Xie. 2022. A convnet for the 2020s. In *Proceedings of the IEEE/CVF conference on computer vision and pattern recognition*. 11976–11986.
- [36] Jiaqi Ma, Tianheng Cheng, Guoli Wang, Qian Zhang, Xinggang Wang, and Lefei Zhang. 2023. Prores: Exploring degradation-aware visual prompt for universal image restoration. *arXiv preprint arXiv:2306.13653* (2023).
- [37] Kede Ma, Wentao Liu, and Zhou Wang. 2015. Perceptual evaluation of single image dehazing algorithms. In *2015 IEEE International Conference on Image Processing (ICIP)*. IEEE, 3600–3604.
- [38] Ningning Liu, Xiangyu Zhang, Hai-Tao Zheng, and Jian Sun. 2018. ShuffleNet v2: Practical guidelines for efficient cnn architecture design. In *Proceedings of the European conference on computer vision (ECCV)*. 116–131.
- [39] Chippy M Manu and KG Sreeni. 2023. GANID: a novel generative adversarial network for image dehazing. *The Visual Computer* 39, 9 (2023), 3923–3936.
- [40] Patrick Morrell. 2024. *Wildfire smoke has led to 'high levels of air pollution' in Toronto, Environment Canada says*. Retrieved April 11, 2024 from <https://www.cbc.ca/news/canada/toronto/special-air-quality-statement-toronto-forest-fire-smoke-1.6866738>
- [41] Ozan Özdenizci and Robert Legenstein. 2023. Restoring vision in adverse weather conditions with patch-based denoising diffusion models. *IEEE Transactions on Pattern Analysis and Machine Intelligence* (2023).
- [42] Dongwon Park, Byung Hyun Lee, and Se Young Chun. 2023. All-in-one image restoration for unknown degradations using adaptive discriminative filters for specific degradations. In *2023 IEEE/CVF Conference on Computer Vision and Pattern Recognition (CVPR)*. IEEE, 5815–5824.
- [43] Vaishnav Potlapalli, Syed Waqas Zamir, Salman Khan, and Fahad Shahbaz Khan. 2023. PromptIR: Prompting for all-in-one blind image restoration. *arXiv preprint arXiv:2306.13090* (2023).
- [44] Mark Sandler, Andrew Howard, Menglong Zhu, Andrey Zhmoginov, and Liang-Chieh Chen. 2018. Mobilenetv2: Inverted residuals and linear bottlenecks. In *Proceedings of the IEEE conference on computer vision and pattern recognition*. 4510–4520.
- [45] Karen Simonyan and Andrew Zisserman. 2015. Very deep convolutional networks for large-scale image recognition. In *3rd International Conference on Learning Representations (ICLR 2015)*.
- [46] Yuda Song, Zhuqing He, Hui Qian, and Xin Du. 2023. Vision transformers for single image dehazing. *IEEE Transactions on Image Processing* 32 (2023), 1927–1941.
- [47] Ziyi Sun, Yunfeng Zhang, Fangxun Bao, Kai Shao, Xinlin Liu, and Caiming Zhang. 2021. IcycleGAN: Single image dehazing based on iterative dehazing model and

929  
930  
931  
932  
933  
934  
935  
936  
937  
938  
939  
940  
941  
942  
943  
944  
945  
946  
947  
948  
949  
950  
951  
952  
953  
954  
955  
956  
957  
958  
959  
960  
961  
962  
963  
964  
965  
966  
967  
968  
969  
970  
971  
972  
973  
974  
975  
976  
977  
978  
979  
980  
981  
982  
983  
984  
985  
986987  
988  
989  
990  
991  
992  
993  
994  
995  
996  
997  
998  
999  
1000  
1001  
1002  
1003  
1004  
1005  
1006  
1007  
1008  
1009  
1010  
1011  
1012  
1013  
1014  
1015  
1016  
1017  
1018  
1019  
1020  
1021  
1022  
1023  
1024  
1025  
1026  
1027  
1028  
1029  
1030  
1031  
1032  
1033  
1034  
1035  
1036  
1037  
1038  
1039  
1040  
1041  
1042  
1043  
1044

1045	CycleGAN. <i>Computer Vision and Image Understanding</i> 203 (2021), 103133.	1103
1046	[48] Christian Szegedy, Wei Liu, Yangqing Jia, Pierre Sermanet, Scott Reed, Dragomir	1104
1047	Anguelov, Dumitru Erhan, Vincent Vanhoucke, and Andrew Rabinovich. 2015.	1105
1048	Going deeper with convolutions. In <i>Proceedings of the IEEE conference on computer</i>	1106
1049	vision and pattern recognition.	1107
1050	[49] Christian Szegedy, Vincent Vanhoucke, Sergey Ioffe, Jon Shlens, and Zbigniew	1108
1051	Wojna. 2016. Rethinking the inception architecture for computer vision. In	1109
1052	<i>Proceedings of the IEEE conference on computer vision and pattern recognition.</i>	1110
1053	2818–2826.	1111
1054	[50] Mingxing Tan, Bo Chen, Ruoming Pang, Vijay Vasudevan, Mark Sandler, Andrew	1112
1055	Howard, and Quoc V Le. 2019. Mnasnet: Platform-aware neural architecture	1113
1056	search for mobile. In <i>Proceedings of the IEEE/CVF conference on computer vision</i>	1114
1057	<i>and pattern recognition.</i> 2820–2828.	1115
1058	[51] Mingxing Tan and Quoc Le. 2019. Efficientnet: Rethinking model scaling for	1116
1059	convolutional neural networks. In <i>International conference on machine learning.</i>	1117
1060	PMLR, 6105–6114.	1118
1061	[52] Yu Xiang Tan, Malika Meghjani, and Marcel Bartholomeus Prasetyo. 2023. Lo-	1119
1062	calization with Anticipation for Autonomous Urban Driving in Rain. (2023).	1120
1063	arXiv:arXiv:2306.09134	1121
1064	[53] Jean-Philippe Tarel, Nicholas Hautiere, Laurent Caraffa, Aurélien Cord, Houssam	1122
1065	Halmaoui, and Dominique Gruyer. 2012. Vision enhancement in homogeneous	1123
1066	and heterogeneous fog. <i>IEEE Intelligent Transportation Systems Magazine</i> 4, 2	1124
1067	(2012), 6–20.	1125
1068	[54] Jean-Philippe Tarel, Nicolas Hautiere, Aurélien Cord, Dominique Gruyer, and	1126
1069	Houssam Halmaoui. 2010. Improved visibility of road scene images under het-	1127
1070	erogeneous fog. In <i>2010 IEEE intelligent vehicles symposium.</i> IEEE, 478–485.	1128
1071	[55] Hayat Ullah, Khan Muhammad, Muhammad Irfan, Saeed Anwar, Muhammad Saj-	1129
1072	jad, Ali Shariq Imran, and Victor Hugo C de Albuquerque. 2021. Light-DehazeNet:	1130
1073	a novel lightweight CNN architecture for single image dehazing. <i>IEEE transactions</i>	1131
1074	<i>on image processing</i> 30 (2021), 8968–8982.	1132
1075	[56] U.S. Department of Transportation, Federal Highway Administration. 2023. <i>Low</i>	1133
1076	<i>Visibility.</i> Retrieved April 11, 2024 from <a href="https://ops.fhwa.dot.gov/weather/weather_events/low_visibility.htm">https://ops.fhwa.dot.gov/weather/</a>	1134
1077	<a href="https://ops.fhwa.dot.gov/weather/weather_events/low_visibility.htm">weather_events/low_visibility.htm</a>	1135
1078	[57] Jeya Maria Jose Valanarasu, Rajeev Yasarla, and Vishal M Patel. 2022. Tran-	1136
1079	sweather: Transformer-based restoration of images degraded by adverse weather	1137
1080	conditions. In <i>Proceedings of the IEEE/CVF Conference on Computer Vision and</i>	1138
1081	<i>Pattern Recognition.</i> 2353–2363.	1139
1082	[58] Tao Wang, Guangpin Tao, Wanglong Lu, Kaihao Zhang, Wenhan Luo, Xiaoqin	1140
1083	Zhang, and Tong Lu. 2024. Restoring vision in hazy weather with hierarchical	1141
1084	contrastive learning. <i>Pattern Recognition</i> 145 (2024), 109956.	1142
1085	[59] Xintao Wang, Ke Yu, Chao Dong, and Chen Change Loy. 2018. Recovering	1143
1086	realistic texture in image super-resolution by deep spatial feature transform. In	1144
1087	<i>Proceedings of the IEEE conference on computer vision and pattern recognition.</i>	1145
1088	606–615.	1146
1089	[60] Yan Yang, Jinlong Zhang, Zhiwei Wang, and Haowen Zhang. 2023. Single image	1147
1090	fast dehazing based on haze density classification prior. <i>Expert Systems with</i>	1148
1091	<i>Applications</i> 232 (2023), 120777.	1149
1092	[61] Mingde Yao, Ruikang Xu, Yuanshen Guan, Jie Huang, and Zhiwei Xiong. 2023.	1150
1093	Neural Degradation Representation Learning for All-In-One Image Restoration.	1151
1094	<i>arXiv preprint arXiv:2310.12848</i> (2023).	1152
1095	[62] Amir Roshan Zamir and Mubarak Shah. 2014. Image geo-localization based	1153
1096	on multiplenearest neighbor feature matching using generalized graphs. <i>IEEE</i>	1154
1097	<i>transactions on pattern analysis and machine intelligence</i> 36, 8 (2014), 1546–1558.	1155
1098	[63] Cheng Zhang, Yu Zhu, Qingsen Yan, Jinqiu Sun, and Yanning Zhang. 2023. All-	1156
1099	in-one multi-degradation image restoration network via hierarchical degradation	1157
1100	representation. In <i>Proceedings of the 31st ACM International Conference on Multi-</i>	1158
1101	<i>media.</i> 2285–2293.	1159
1102	[64] Yuxiao Zhang, Alexander Carballo, Hanqing Yang, and Kazuya Takeda. 2023.	1160
	Perception and sensing for autonomous vehicles under adverse weather condi-	
	tions: A survey. <i>ISPRS Journal of Photogrammetry and Remote Sensing</i> 196 (2023),	
	146–177.	
	[65] Yuan Zhang, Youpeng Sun, Zheng Wang, and Ying Jiang. 2023. YOLOv7-RAR for	
	urban vehicle detection. <i>Sensors</i> 23, 4 (2023), 1801.	
	[66] Bolei Zhou, Hang Zhao, Xavier Puig, Sanja Fidler, Adela Barriuso, and Antonio	
	Torralba. 2017. Scene parsing through ade20k dataset. In <i>Proceedings of the IEEE</i>	
	<i>conference on computer vision and pattern recognition.</i> 633–641.	
	[67] Bolei Zhou, Hang Zhao, Xavier Puig, Tete Xiao, Sanja Fidler, Adela Barriuso, and	
	Antonio Torralba. 2019. Semantic understanding of scenes through the ade20k	
	dataset. <i>International Journal of Computer Vision</i> 127, 3 (2019), 302–321.	